

Rethinking Weak-to-Strong Augmentation in Source-Free Domain Adaptive Object Detection

Jiuzheng Yang¹, Song Tang^{1,2*}, Yangkuiyi Zhang¹, Shuaifeng Li³,
Mao Ye³, Jianwei Zhang², and Xiatian Zhu⁴

¹University of Shanghai for Science and Technology ²Universität Hamburg
³University of Electronic Science and Technology of China ⁴University of Surrey
eason1337@gmail.com, tangs@usst.edu.cn, maoye@uestc.edu.cn, xiatian.zhu@surrey.ac.uk

Abstract

Source-Free domain adaptive Object Detection (SFOD) aims to transfer a detector (pre-trained on source domain) to new unlabelled target domains. Current SFOD methods typically follow the Mean Teacher framework, where weak-to-strong augmentation provides diverse and sharp contrast for self-supervised learning. However, this augmentation strategy suffers from an inherent problem called *crucial semantics loss*: Due to random, strong disturbance, strong augmentation is prone to losing typical visual components, hindering cross-domain feature extraction. To address this thus-far ignored limitation, this paper introduces a novel **Weak-to-Strong Contrastive Learning (WSCoL)** approach. The core idea is to distill semantics lossless knowledge in the weak features (from the weak/teacher branch) to guide the representation learning upon the strong features (from the strong/student branch). To achieve this, we project the original features into a shared space using a mapping network, thereby reducing the bias between the weak and strong features. Meanwhile, a weak features-guided contrastive learning is performed in a weak-to-strong manner alternatively. Specifically, we first conduct an adaptation-aware prototype-guided clustering on the weak features to generate pseudo labels for corresponding strong features matched through proposals. Sequentially, we identify positive-negative samples based on the pseudo labels and perform cross-category contrastive learning on the strong features where an uncertainty estimator encourages adaptive background contrast. Extensive experiments demonstrate that WSCoL yields new state-of-the-art performance, offering a built-in mechanism mitigating crucial semantics loss for traditional Mean Teacher framework. The code and data will be released soon.

Introduction

In recent years, there have been significant advancements in image object detection using deep convolutional neural networks, such as YOLO (Bochkovskiy, Wang, and Liao 2020) and Faster R-CNN (Ren et al. 2015). However, when these networks are exposed to new environments, such as changes in weather or illumination (domain shift), their performance often degrades significantly. Within this context, in line with the current focus on data privacy, distributed storage, and transmission limitations, a practical setting, known as “*Source-Free domain adaptive Object Detection*” (SFOD) (Li

*Corresponding author

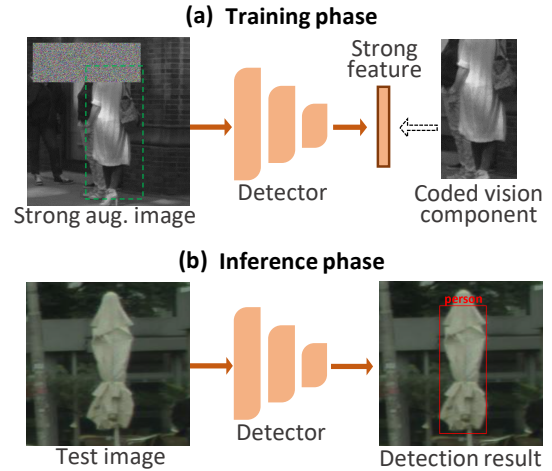


Figure 1: Illustration of *crucial semantics loss* problem. (a) Strong augmentation may lose typical visual components, e.g., head, leading to encode discriminative-less part, e.g., body with a skirt. Thus, the learned cross-domain features cannot apply to some scenarios, such as containing an umbrella, as shown in (b).

et al. 2021), has gained attention. Unlike the conventional Un-supervised Domain Adaptation (UDA) setting, SFOD aims to transfer detection models pre-trained on the source domain to a distinct but related unlabeled target domain, without requiring access to labeled source data.

The current mainstream for the SFOD problem is the Mean-Teacher (Tarvainen and Valpola 2017) approach, which applies different augmentations/noise to the student model and teacher model with Exponential Moving Average (EMA) updating and achieves model training using self-supervised learning, e.g., semantic consistency. The existing methods extend this framework from different views. For instance, inspired by the UDA work, the adversarial learning (Xiong et al. 2021; Chu et al. 2023; Deng, Li, and Duan 2024) is introduced to extract cross-domain features; the contrastive learning (VS, Oza, and Patel 2023; Chen, Wang, and Zhang 2023) is exploited to refine the discriminative features. In those work, the *weak-to-strong augmentation* is the dominant augmentation strategy, resulting in rich and sharp contrast.

Although this weak-to-strong scheme significantly pro-

motes extracting the domain-invariant features, it has an inherent limitation: *The strong augmentation is prone to lose the typical visual components* due to random strong disturbing such as mosaic, color jittering, and blurring, making it difficult to achieve high-quality cross-domain representation. For example, as shown in Fig. 1 (a), given that a head is the most discriminative part of persons, if the head is mosaicked, the learned features attached to the person category may converge to the body with white skirt. Consequently, as encountering a new domain containing a white umbrella, the adapted detector may confuse person with the umbrella (Fig. 1 (b)). Unfortunately, the issue is thus-far ignored by the existing work, highlighting the need for a built-in design for this problem that we call it as “*crucial semantics loss*” in this paper.

To address the limitation above, in this paper, we propose a new **Weak-to-Strong Contrastive Learning (WSCoL)** approach. Our idea is grounded on the fact that the weak augmentation does not suffer the crucial semantics loss problem since the used transformations, such as re-sizing and flipping, don’t greatly change image content. Thus, we dynamically mine semantics lossless information from the weak features (from the weak branch) to regulate the representation learning on the strong features (from the strong branch). Specifically, to account for the large discrepancy between the weak and strong features, we employ a mapping network to project them to the learnable bias-less feature space. Our contrastive learning follows a weak-to-strong pipeline. Freezing the mapping network, we first carry out an adaptation-aware prototype-guided clustering on the weak features to generate pseudo labels for the corresponding strong features¹, in which the EMA updated prototypes capture the dynamics of the adaptation process. Sequentially, with the unfrozen mapping network, a cross-category contrastive learning on the strong features is performed based on the positive-negative samples partition specified by the pseudo labels obtained early. In addition, we develop an uncertainty estimation module to encourage adaptive background contrasting.

Our **contributions** are summarized as follow: **(1)** This work is the initial attempt to address the crucial semantics loss problem of weak-to-strong augmentation in the SFOD context. **(2)** To address this problem, we propose a new WSCoL approach that performs a weak features-guided contrastive learning over the strong features in a bias-less feature space. **(3)** We conduct extensive evaluation experiments on seven standard datasets. The results confirm that WSCoL can achieve state-of-the-art performance compared to previous alternatives.

Related Work

Unsupervised Domain Adaptive Object Detection. Recent advancements in Unsupervised Domain Adaptive Object Detection (UDAOD) have introduced various strategies that rely on access to source data (the difference from SFOD). Methods are roughly classified into five strategies. The first is adversarial feature learning (Chen et al. 2018; Saito et al.

¹The corresponding relationship is grounded on the fact that all features are tailored by the same teacher proposals (see Fig. 2).

2019; Hsu et al. 2020a; Sindagi et al. 2020; Vs et al. 2021), using gradient reversal layers as in DANN (Ganin et al. 2016). The second involves pseudo-labeling (Inoue et al. 2018; Roy-Chowdhury et al. 2019; Khodabandeh et al. 2019), using high-confidence predictions to train the target domain. The third is image-to-image translation (Zhang et al. 2019; Hsu et al. 2020b; Chen et al. 2020a; Rodriguez and Mikolajczyk 2019), converting images between domains using unpaired translation models. The fourth is domain randomization (Kim et al. 2019; Rodriguez and Mikolajczyk 2019), generates multiple stylized versions of source data for robust training. The fifth is Mean-Teacher training (Deng et al. 2021; Cai et al. 2019), which improves generalization by incrementally training with unlabeled data. Despite these advancements, all methods still rely on access to source domain data.

Source-Free Domain Adaptation. *Source-Free Domain Adaptation* (SFDA) is more challenging than traditional UDA due to total absence of both source and target data, involving classification and detection tasks. Existing SFDA methods for classification task can be grouped into three categories. The first category converts the SFDA problem into a UDA problem by creating a pseudo-source domain (Li et al. 2020b; Tian et al. 2021) or segmenting the target domain into source-like subsets (Du et al. 2021). The second approach leverages auxiliary information from the pre-trained source model, such as multiple hypotheses (Lao, Jiang, and Havaii 2020), prototypes (Tanwisuth et al. 2021; Zhou et al. 2024) to align source and target features. The third approach focuses on generating robust pseudo-labels by applying techniques like domain-aware gradient control (Yang et al. 2021), target data manifolds (Tang et al. 2022, 2024a) and foundation multi-modal model guiding (Tang et al. 2024b).

Most SFDA methods for detection task (also known in SFOD) follow a self-training paradigm, broadly categorized into three approaches. The first approach focuses on obtaining higher quality pseudo-labels by setting thresholds through self-entropy descent (Li et al. 2021) or balancing classes (Deng, Li, and Duan 2024). The second approach treats target domain images as separate domains by utilizing different variances or augmentations and extracts domain-invariant features via graph-based alignment (Li et al. 2022) or adversarial learning (Xiong et al. 2021; Chu et al. 2023). The third approach enhances object representation by contrastive learning via instance relation graph (VS, Oza, and Patel 2023) or adjacent proposals (Chen, Wang, and Zhang 2023). However, these methods above lack built-in design addressing the issue of crucial semantics loss.

Methodology

Problem statement. Suppose the source domain $\mathcal{D}_s = \{(I_i^s, Y_i^s)\}_{i=1}^{N_s}$ is labeled, where $Y_i^s = \{(b_j^s, c_j^s)\}_j^{M_s}$ denote the boxes and classes of the objects in the i -th source image I_i^s , M_s denote the total number of object in I_i^s , and N_s stands for the total number of source images. The target domain $\mathcal{D}_t = \{x_i\}_{i=1}^{N_t}$ is unlabeled, where N_t denotes the total number of target images and the target samples obey the same distribution. Our goal is to transfer the source detection

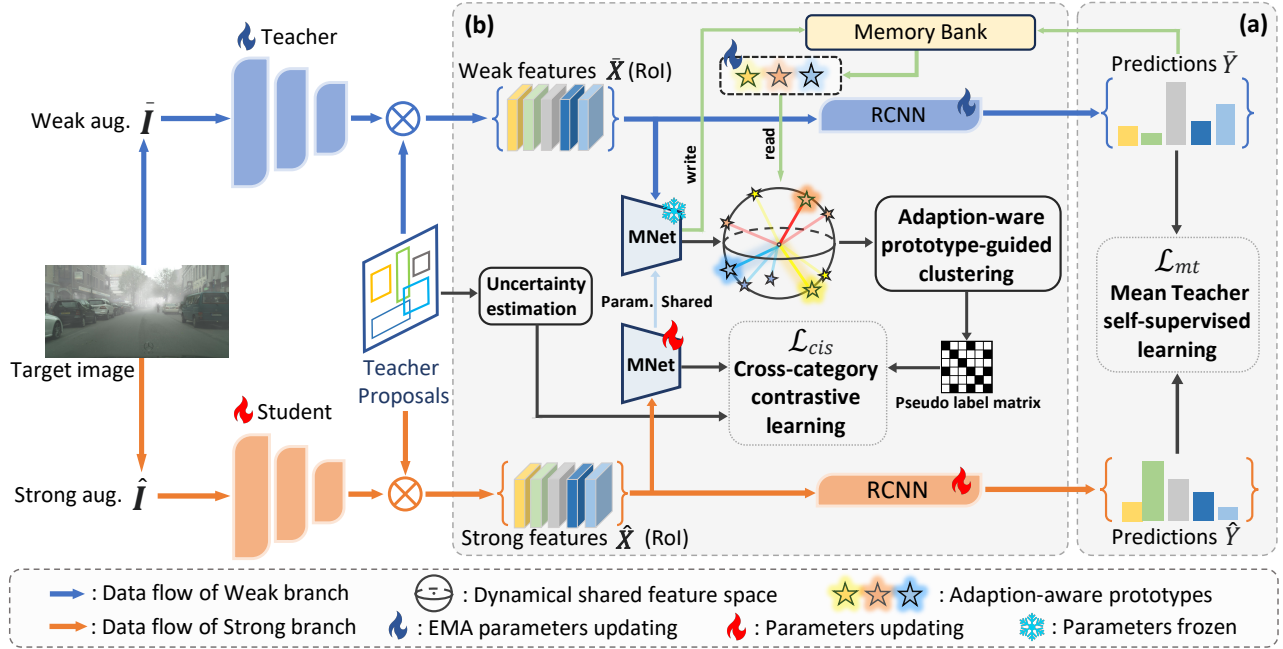


Figure 2: Overview of WSCoL. Building upon (a) the self-supervised learning between predictions \bar{I} and \hat{I} as classic Mean Teacher approach, WSCoL conducts (b) a cross-category contrastive learning with uncertainty estimation over the strong features \hat{X} with guidance clustered from the weak features \bar{X} (distilled by the adaptation-ware prototype-guided clustering). Additionally, a mapping network (MNet) learns a shared space for this contrastive learning, decreasing the semantics shift between \bar{X} and \hat{X} .

model pre-trained on \mathcal{D}_s to the target domain \mathcal{D}_t . During the adaptation, \mathcal{D}_t is available while \mathcal{D}_s cannot be accessed.

Overview. The proposed WSCoL method is built upon the popular Mean Teacher framework. As shown in Fig. 2, our model consists of the weak and strong branches that serve as the teacher and student models, respectively. Both branches' structures are based on Faster-RCNN and initialized as the source model. Specifically, in the strong branch, the image with strong augmentation \hat{I} is first converted to image feature by a deep architecture and further to M strong (RoI) features $\hat{X} = \{\hat{x}_i\}_{i=1}^M$ (i.e., strong features) tailored by the teacher proposals (generated by RPN in the weak branch). Lastly, RCNN module outputs predictions $\hat{Y} = \{\hat{b}_i, \hat{c}_i\}_{i=1}^M$ for the strong features where \hat{b}_i and \hat{c}_i are the bboxes and category distribution of the i -the instance in \hat{I} . The weak branch is the same as the strong one, except for two points: image input with weak augmentation, and EMA updating based on the strong branch. As the weak-augmented image \bar{I} goes through the weak branch, we obtain M weak (RoI) features $\bar{X} = \{\bar{x}_i\}_{i=1}^M$ and their predictions $\bar{Y} = \{\bar{b}_i, \bar{c}_i\}_{i=1}^M$.

The conventional Mean Teacher approach involves a form of self-supervised learning, which is regularized by \mathcal{L}_{mt} (elaborated in the next subsection). Our WSCoL method serves as a plug-in module, including (I) mapping network (denoted by MNet), (II) adaptation-ware prototype-guided clustering, and (III) cross-category contrastive learning with uncertainty estimation. In the proposed method, MNet learns a shared space that reduces the

bias between the weak and strong features; the clustering distills the lossless knowledge from the weak features, while the contrastive learning upon the strong features (\mathcal{L}_{cis}) promotes extracting cross-domain representations.

Mean Teacher Objective

Mean Teacher approach performs a self-supervised learning. Suppose $\bar{Y}^h = \{\bar{b}_i^h, \bar{c}_i^h\}_{i=1}^M$ be the predictions of high confident instances in the weak branch's predictions \bar{Y} . The Mean Teacher objective can be:

$$\begin{aligned} \mathcal{L}_{mt} &= \mathcal{L}_{det}(\hat{I}, \bar{Y}^h) + \mathcal{L}_{con}(\hat{I}, \bar{Y}) \\ \mathcal{L}_{det}(\hat{I}, \bar{Y}^h) &= \mathcal{L}_{rpn}(\hat{I}, \bar{b}^h) + \mathcal{L}_{rcnn}(\hat{I}, \bar{a}^h) \\ \mathcal{L}_{con}(\hat{I}, \bar{Y}) &= \frac{1}{M} \sum D_{KL}(\hat{c}_i || \bar{c}_i), \end{aligned} \quad (1)$$

where $\sum D_{KL}$ is the Kullback–Leibler divergence function; \bar{a}^h is the one-hot version of \bar{c}^h . In Eq. (1), \mathcal{L}_{con} presents a semantic consistency regularization between the matched instance-pairs tailored by the same teacher proposal. \mathcal{L}_{det} derives from the Fater-RCNN paradigm, consisting of location regression term (\mathcal{L}_{rpn}) and classification term (\mathcal{L}_{rcnn}). To exclude the noise in \bar{Y} , only credible predictions \bar{Y}^h are treated as pseudo labels.

Weak-to-Strong Contrastive Learning

As the mentioned in overview, our method involves the three modules below.

I. Mapping network. Although generating sharp contrasts, the weak-to-strong augmentation strategy also leads to extra semantic shift/bias between the weak and strong features. This shift will decrease the credibility of distilled information from the weak features. To tackle this issue, we employ MNet to project original features into a shared space, thereby reducing the shift.

Specifically, MNet consists of three consecutive blocks including a BN layer-ending and a convolutional layer (without padding), followed by three full-connected layers (the details are provided in Supplementary). After MNet mapping, any weak features \bar{x}_i and strong features \hat{x}_i are converted to

$$\bar{z}_i = \Theta_{\text{MNet}}(\bar{x}_i), \quad \hat{z}_i = \Theta_{\text{MNet}}(\hat{x}_i), \quad (2)$$

where Θ_{MNet} is the parameters of MNet. Of note, to mitigate losing the crucial visual components, we tailor those features using the teacher proposals generated by the weak branch.

Remark. As demonstrated in Fig. 2, MNet serves for both branches in different ways. Specifically, MNet is jointly trained with the strong branch, while it is frozen as working for the weak branch. This alternative way encourages a gradual search for the optimal shared space. In addition, MNet only works during the training phase while being removed as the inference time.

II. Adaptation-aware prototype-guided clustering. To account for the unsupervised setting, we adopt clustering to mine the useful category information. In the SFOD context, it is challenging to perform a global clustering on diverse and number-varying instance features, due to dynamical proposals predictions. To address this challenge, we perform the adaptation-aware prototype-guided clustering based on a memory bank storing historical information. In each training iteration, this clustering consists of two phases below.

Adaptation-aware prototypes discovery. Suppose the memory bank is a queue bundle that contains K queues with D size, in which K is the number of object categories of the training dataset, D is the storage length. We collectively write them to $\mathcal{M} \in \mathbb{R}^{K \times D}$. For the k -th category ($k \in K$), the prototype in iteration t , denoted by \mathcal{P}_k^t , is computed as

$$\mathcal{P}_k^t = (1 - \eta)\mathcal{P}_k^{t-1} + \eta \frac{1}{D} \sum_{i=1}^D \Theta_{\text{MNet}}(\mathcal{M}_{k,i}), \quad (3)$$

where $\eta < 1$, $\mathcal{M}_{k,i}$ is the i -th element in the k -th row \mathcal{M}_k . As depicted in Eq. (3), \mathcal{P}_k^t is updated in the EMA fashion, thereby the dynamics of adaptation are captured. Regarding updating the memory bank, for each category, we use the Top-D weak features with high confidence to update the bank \mathcal{M} , according to the weak branch’s predictions \bar{Y}^h .

Unlike previous methods, we treat the background as the $(K + 1)$ -th independent category and its prototype is discovered by an online weighted clustering. As stated early, the weak branch generates weak feature $\bar{X} = \{\bar{x}_i\}_{i=1}^M$ for the weak-augmented image \bar{I} , and their predictions are $\bar{Y} = \{\bar{b}_i, \bar{c}_i\}_{i=1}^M$. The computation of background prototype can be formulated as:

$$\mathcal{P}_{K+1} = \frac{\sum_{\bar{x}_i \in \bar{X}} (\delta_{K+1}(\bar{c}_i) \bar{z}_i)}{\sum_{\bar{x}_i \in \bar{X}} \delta_{K+1}(\bar{c}_i)}, \quad (4)$$

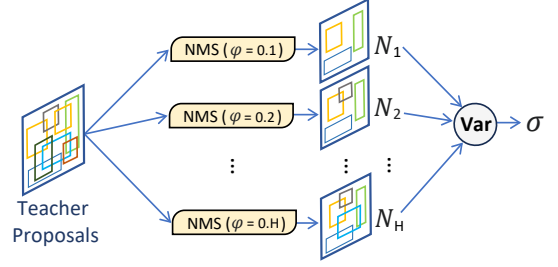


Figure 3: Illustration of proposal-based uncertainty estim..

where softmax function $\delta_{K+1}(\cdot)$ return the $(K + 1)$ -th element of the output vector, \bar{z}_i is the mapped feature of \bar{x}_i .

Pseudo labels generation. Given that the prototypes provide a classification bases, we implement the classification for the mapped features using similarity comparison in the two rounds below.

Round 1: Obtain prototypes-based pseudo label for \bar{z}_i by the nearest centroid measurement:

$$\bar{p}_i = \arg \min_j D_{\text{cos}}(\bar{z}_i, \mathcal{P}_j), \quad (5)$$

where D_{cos} computes the cosine distance of the two inputs.

Round 2: Obtain final pseudo label for \bar{z}_i by weighted clustering.

$$\begin{aligned} \mathbf{o}^k &= \frac{\sum_{\bar{x}_i \in \bar{X}} (\mathbb{I}_{[\bar{p}_i=1]} \bar{z}_i)}{\sum_{\bar{x}_i \in \bar{X}} \mathbb{I}_{[\bar{p}_i=1]}}, \quad k \in [1, K + 1]; \\ \bar{y}_i &= \arg \min_j D_{\text{cos}}(\bar{z}_i, \mathbf{o}^k), \end{aligned} \quad (6)$$

where $\mathbb{I}_{[\bar{p}_i=1]}$ is the indicator function, \mathbf{o}^k is the k -th clustering centroid. As mentioned above, our pseudo label generation integrates the information from both prototypes (Eq. (5)) and the self-mapped features (Eq. (6)).

Remark: We don’t create the background prototype using the EMA method (Eq. (3)) for the following reason. Unlike natural categories like cars and pedestrians, the background is a comprehensive category that typically contains multiple subcategories. For example, in traffic scenarios, a flowerpot and a pig both belong to the background. It’s difficult to find commonalities between them. Within this context, considering historical background information may lead to more multiple subcategories, making it hard to converge to a robust commonality representation. To mitigate this issue, we only utilize the current features to create the clustering-based prototype, capturing the current image-specific visual clues in the background.

III. Cross-category contrastive learning Conventional contrastive learning (He et al. 2020; Chen et al. 2020b) works in the instance manner: For a given sample, its augmented one is the positive data while other samples are negative data. Our scheme focuses on contracting different categories, namely constructing the positive and negative partition based on the clustering-based pseudo labels. Furthermore, given that unlike the classification problem, a detection task-specific challenge is utilizing the background properly. Here, we estimate the prediction uncertainty of the input image to achieve reasonable utilization of semantics in the background.

Algorithm 1: Training of WSCoL

Input: Unlabeled target domain \mathcal{D}_t , Source model Θ_s , target dataset \mathcal{X}_t , mapping network Θ_{MNet}

- 1: **Initialisation:** Set weak (teacher) and strong (student) branches $\Theta_{wa} = \Theta_{sa} = \Theta_s$, initialize Θ_{MNet} randomly.
- 2: **for** $m = 0 \rightarrow EpochNum$ **do**
- 3: Update Θ_{wa} in a EMA manner;
- 4: **for** $t = 0 \rightarrow IterNum$ **do**
- 5: Sample a target image I from \mathcal{D}_t ;
- 6: Generate weak and strong features \bar{X} , \hat{X} and their predictions \hat{Y} , \bar{Y} by inputting I into Θ_{wa} and Θ_{sa} , respectively;
- 7: Fix Θ_{MNet} and generate pseudo labels for \hat{X} using the adaptation-aware prototype-guided clustering on \bar{X} (Eq. (3), (4), (5), (6));
- 8: Estimate prediction uncertainty of I (Eq. (7));
- 9: Update Θ_{sa} and Θ_{MNet} by optimizing objective L_{WSCoL} (Eq. (10)) over \hat{X} .
- 10: **end for**
- 11: **end for**
- 12: **return** Adapted Θ_{sa} model.

Proposals-based uncertainty estimation. We develop an intuitive strategy to implement uncertainty estimation. To be concrete, we apply the Non-Maximum Suppression (NMS) operation on the teacher proposals for H times where IoU threshold is set to $\varphi = 0.1 \sim 0.H$, respectively. The estimation is achieved by calculating the variance of the NMS results, denoted by $N_1 \sim N_H$, as:

$$\sigma = \text{Var}(\bar{I}) = \frac{1}{H} \sum_{i=1}^H (N_i - \mu)^2, \quad (7)$$

where μ is the mean value of $N_1 \sim N_H$.

Loss with adaptive background contrast. Our contrastive loss adopts a form similar to SupCon (Khosla et al. 2020). Suppose for the mapped feature of any strong feature, \hat{z}_i , its positive data are the ones in strong features \hat{X} with the same category as \hat{z}_i , whose mapped features is denoted by \mathcal{G}_i . Accordingly, others in \hat{X} are the negative data, whose mapped features are written as \mathcal{V}_i collectively. The contrastive loss becomes:

$$\mathcal{L}_{abc} = -\frac{1}{|\hat{X}|} \sum_{\hat{z}_i \in \hat{X}} \sum_{\hat{z}_j \in \mathcal{G}_i} \log \frac{\exp(\hat{z}_i \cdot \hat{z}_j / \tau)}{\sum_{\hat{z}_k \in \mathcal{V}_i} \exp(\hat{z}_i \cdot \hat{z}_k / \tau)}, \quad (8)$$

where τ is the temperature parameter; \mathcal{V}_i is adaptive to the prediction uncertainty of the input image by the rule:

$$\mathcal{V}_i = \begin{cases} \mathcal{V}_{obj} & (\sigma > u) \\ \mathcal{V}_{obj} \cup \mathcal{V}_{bg} & (\sigma \leq u) \end{cases}, \quad (9)$$

where u is a threshold; \mathcal{V}_{obj} and \mathcal{V}_{bg} are formed by the features assigned with object category and background category, respectively.

Remark. With accurate category information, introducing background semantics can boost contrastive learning.

		Cityscapes \rightarrow FoggyCityscapes									
Methods	Venue	SF	Pson	Rder	Car	Tuck	Bus	Tain	Mcle	Bcle	mAP
Source	-	-	31.1	38.5	36.1	19.8	23.5	9.1	21.8	30.5	26.3
DAF	CVPR'18	\times	25.0	31.0	40.5	22.1	35.3	20.2	20.0	27.1	27.6
SWDA	CVPR'19	\times	29.9	42.3	43.5	24.5	36.2	32.6	30.0	34.8	34.3
MTOR	CVPR'19	\times	30.6	41.4	44.0	21.9	38.6	28.0	23.5	35.6	35.1
SCDA	CVPR'19	\times	33.8	42.1	52.1	26.8	42.5	26.5	29.2	34.5	35.9
UMT	CVPR'21	\times	33.8	47.3	49.0	28.0	48.2	42.1	33.0	37.3	40.4
MeGA	CVPR'21	\times	37.7	49.0	49.4	25.4	46.9	34.5	34.5	39.0	41.8
SED	AAAI'21	\checkmark	33.2	40.7	44.5	25.5	39.0	22.2	28.4	34.1	33.5
SOAP	PR'21	\checkmark	35.9	45.0	48.4	23.9	37.2	24.3	31.8	37.9	35.5
LODS	CVPR'22	\checkmark	34.0	45.7	48.2	27.3	39.7	19.6	32.3	37.8	35.8
A ² SFOD	AAAI'23	\checkmark	32.3	44.1	44.6	28.1	34.3	29.0	31.8	38.9	35.4
PETS	ICCV'23	\checkmark	42.0	48.7	56.3	19.3	39.3	5.5	34.2	41.6	35.9
IRG	CVPR'23	\checkmark	37.4	45.2	51.9	24.4	39.6	25.2	31.5	41.6	37.1
LPU	ACMMM'23	\checkmark	39.0	50.3	55.4	24.0	46.0	21.2	30.3	44.2	38.8
BT	TCSVT'24	\checkmark	38.4	47.1	52.7	24.3	44.6	36.3	30.2	40.1	39.5
WSCoL	-	\checkmark	37.1	47.6	52.2	30.7	45.7	37.3	31.4	42.8	40.6
Oracle	-	-	38.7	46.9	56.7	35.5	49.4	44.7	35.9	38.8	43.1

Table 1: Results on **Cityscapes \rightarrow FoggyCityscapes**. SF means source-free.

However, in the scenarios lacking effective supervision, e.g., SFOD, the background information often contains much noise, deteriorating the contrastive performance. Thus, we design the uncertainty-based adaptive mechanism as Eq. (9) to balance effect of the background.

IV. Overall objective and model training

As aforementioned, our method extends the Mean-Teacher framework. Combining Eq. (1) and Eq. (8), the objective of WSCoL is formulated by Eq. (10).

$$\mathcal{L}_{WSCoL} = \min_{\Theta} \mathcal{L}_{mt} + \alpha \mathcal{L}_{abc} \quad (10)$$

where α is a trade-off hyper-parameter; $\Theta = \{\Theta_{sa}, \Theta_{MNet}\}$ is parameters of models from the strong branch, in which Θ_{sa} stands for the parts except for Θ_{MNet} . During the model training, we optimize the strong branch iteration-wise, while the EMA updating on the weak branch is triggered epoch-wise. The concrete training is presented in Alg. 1.

Experiments

Dataset. We evaluated our method on seven datasets in total: **Cityscapes** (Cordts et al. 2016), **Foggy-Cityscapes** (Sakaridis, Dai, and Van Gool 2018) (we use only the most severe foggy condition 0.02.), **Pascal** (Everingham et al. 2010), **Clipart** (Inoue et al. 2018), **Watercolor** (Inoue et al. 2018), **KITTI** (Geiger et al. 2013) and **Sim10K** (Johnson-Roberson et al. 2016). The details of the seven datasets are provided in Supplementary.

Domain adaptation settings. Upon the seven datasets, five transfer tasks is built belonging to two scenarios: **(1) City Scene Adaptation:** Cityscapes \rightarrow FoggyCityscapes, Sim10k \rightarrow Cityscapes, and KITTI \rightarrow Cityscapes; **(2) Image Style Adaptation:** Pascal \rightarrow Watercolor and Pascal \rightarrow Clipart.

Method	Venue	SF	Sim10K \rightarrow City	KITTY \rightarrow City
			AP on car	AP on car
Source	-	-	33.3	34.6
DAF	CVPR'18	✗	38.9	38.5
SWDA	CVPR'19	✗	40.1	37.9
SCDA	CVPR'19	✗	43.0	42.5
UMT	CVPR'21	✗	43.1	-
MeGA	CVPR'21	✗	44.8	43.0
SED	AAAI'21	✓	43.1	44.6
SOAP	PR'21	✓	41.6	42.7
LODS	CVPR'22	✓	-	43.9
A ² SFOD	AAAI'23	✓	44.0	44.9
IRG	CVPR'23	✓	45.2	46.9
LPU	ACMMM'23	✓	48.4	47.3
BT	TCSVT'24	✓	48.6	48.7
WSCoL	-	✓	49.5	50.7

Table 2: Results on **Sim10k \rightarrow Cityscapes** and **KITTY \rightarrow Cityscapes**.

Implementation details. For the sake of fairness, our experimental settings is the same as the previous work (Li et al. 2022; VS, Oza, and Patel 2023; Deng, Li, and Duan 2024) that are elaborated in Supplementary.

Comparison with state-of-the-art methods

To evaluate the effectiveness of WSCoL, we select 18 comparisons divided into three categories. *The first category* contains Source and Oracle models that denote Faster R-CNN trained on source domain data and target domain data using real labels, respectively, using real labels. The two models specify the upper and lower bounds of transfer performance. *The second category* is 8 SFOD methods, including SED (Li et al. 2021), SOAP (Xiong et al. 2021), LODS (Li et al. 2022), A²SFOD (Chu et al. 2023), IRG (VS, Oza, and Patel 2023), LPU (Chen, Wang, and Zhang 2023), PETS (Liu et al. 2023) and Balance Teacher (BT) (Deng, Li, and Duan 2024). *The last one* is 8 UDAOD methods, including DA-Faster (Chen et al. 2018), SWDA (Saito et al. 2019), MTOR (Cai et al. 2019), SCDA (Zhu et al. 2019), MeGA (Vs et al. 2021), SAPNet (Li et al. 2020a), PD (Wu et al. 2021) and UMT (Deng et al. 2021). The results are cited from their original papers.

Main results. The results on the transfer tasks are presented in Tab. 1~Tab. 3. In the first scenario, WSCoL improved by **1.1%**, **0.9%**, and **2.0%** in the task Cityscapes \rightarrow FoggyCityscapes, Sim10k \rightarrow Cityscapes, and KITTY \rightarrow Cityscapes, respectively, compared with the previous best method BT. In the second scenario, WSCoL outperforms the second-best method BT and LODS by **0.8%** and **1.2%** on the task Pascal \rightarrow Watercolor and Pascal \rightarrow Clipart, respectively. Compared to UDAOD methods, WSCoL also achieves superior performance. Compared with the second-best MeGA (the first scenario) and UMT (the second scenario), WSCoL improves by **0.2%** and **2.3%** at least, respectively.

Qualitative comparison. As a toy example, in Fig. 4, we visualize the detection results from Cityscapes \rightarrow FoggyCityscapes, taking IRG (VS, Oza, and Patel 2023) as comparison. Obviously, our method is able to detect more objects while maintaining accuracy. Especially in foggycityscaps,

Methods	Venue	SF	Pascal \rightarrow Watercolor					P \rightarrow C		
			bike	bird	car	cat	dog	prsn	mAP	mAP
Source	-	-	70.8	46.4	47.7	30.4	29.8	53.8	46.5	28.6
SWDA	CVPR'19	✗	82.3	55.9	46.5	32.7	35.5	66.7	53.3	38.1
SAPNet	ECCV'20	✗	81.1	51.1	53.6	34.3	39.8	71.3	55.2	42.2
PD	TPAMI'21	✗	95.8	54.3	48.3	42.4	35.1	65.8	56.9	42.1
UMT	CVPR'21	✗	88.2	55.3	51.7	39.8	43.6	69.9	58.1	44.1
SOAP	PR'21	✓	79.3	44.3	41.4	45.7	39.3	55.9	51.0	29.9
LODS	CVPR'22	✓	95.2	53.1	46.9	37.2	47.6	69.3	58.2	45.2
IRG	CVPR'23	✓	75.9	52.5	50.8	30.8	38.7	69.2	53.0	31.5
BT	TCSVT'24	✓	89.3	56.4	54.9	40.4	46.0	72.5	59.9	-
WSCoL	-	✓	84.8	55.6	55.8	47.8	49.0	71.5	60.7	46.4

Table 3: Results on **Pascal \rightarrow Watercolor** and **Pascal \rightarrow Clipart** (denote P \rightarrow C in short); the full results on **Clipart** are in Supplementary.

#	Methods	Losses			mAP	
		\mathcal{L}_{det}	\mathcal{L}_{con}	\mathcal{L}_{abc}	Foggy	water
1	Source Only	✗	✗	✗	26.3	46.5
2	-	✓	✗	✗	36.2	56.6
3	WSCoLw/o \mathcal{L}_{cis}	✓	✓	✗	37.2	57.2
4	WSCoLw/o \mathcal{L}_{con}	✓	✗	✓	38.9	60.5
5	WSCoL	✓	✓	✓	40.6	60.7
6	WSCoLw/o MNet				38.7	58.7
7	WSCoLw/o UnEst				39.8	59.9

Table 4: Ablation study results on **Cityscapes \rightarrow FoggyCityscapes** and **Pascal \rightarrow Watercolor**.

even if some objects are heavily obscured by fog, our method can still accurately detect them. More visualization results are provided in Supplementary.

Ablation Study

To evaluate the contributions of different components in our model, we perform ablation studies on the tasks Cityscapes \rightarrow FoggyCityscapes and Pascal \rightarrow Watercolor. The results are shown in Tab. 4.

Effect of objective components For a comprehensive comparison, we isolate the effect of three components in \mathcal{L}_{WSCoL} . As shown in Tab. 4, the evident performance drops (compared to WSCoL) in 3, 4 row confirm the effect of \mathcal{L}_{abc} and \mathcal{L}_{con} . Moreover, removing \mathcal{L}_{abc} results in a larger decrease than removing \mathcal{L}_{con} , implying stronger impact of \mathcal{L}_{abc} .

Effect of mapping network and uncertainty estimation.

To evaluate the two moduls, we propose two variations of WSCoL. Specifically, WSCoL w/o MNet removes MNet and conducts our contrastive learning on original weak and strong features, while WSCoL w/o UnEst blindly takes the background as contrasting. As shown in Tab. 4 (6, 7 row), mAP of WSCoL w/o MNet decreases to **38.7%** on FoggyCityscapes and **58.7%** on Watercolor. Removing uncertainty estimation led to mAP reduction by **0.8%** and **0.6%**, respectively, compared to WSCoL. These results confirm the importance of



Figure 4: Quantitative results of IRG and our WSCoL on task Cityscapes \rightarrow FoggyCityscapes. Green, blue and red boxes represent true positives (TP), false positives (FP), and false negatives (FN) respectively. *Zoom in for best view.*

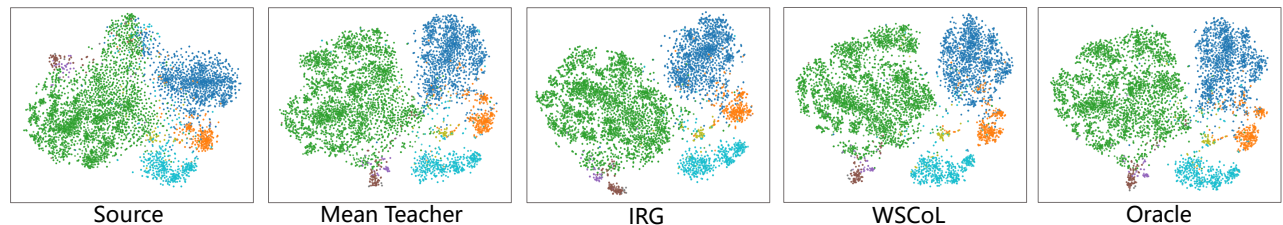


Figure 5: Feature distribution visualization on task Cityscapes \rightarrow FoggyCityscapes. Categories are presented in different colors.

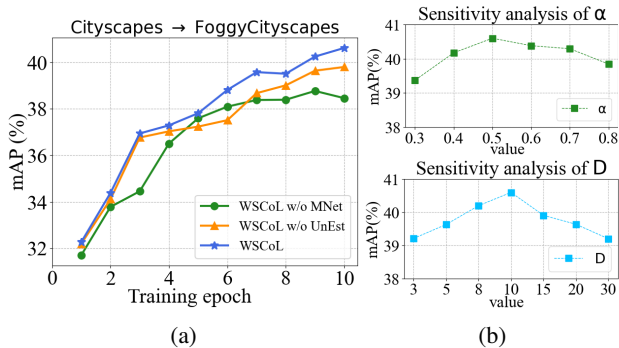


Figure 6: Model analysis. (a) Illustration of training dynamics. (b) mAP varying as α (Top) and D (Bottom) changing.

each component in achieving optimal performance.

Further Analysis

Feature distribution visualization. We employed t-SNE to visualize the feature distribution using the test images on task Cityscapes \rightarrow FoggyCityscapes. Meanwhile, the source model (denoted as Source), Mean Teacher (trained by \mathcal{L}_{mt}), IRG and Oracle (trained on FoggyCityscapes with ground truth) are selected as comparisons. As illustrated in Fig. 5, from Source to WSCoL, the aggregation becomes obvious gradually. Notably, WSCoL’s distribution shape closely resembles that of Oracle.

Training dynamics. A robust training is crucial for self-supervised learning-based methods. In this part, we present the training dynamics of WSCoL, while WSCoL w/o Mnet

and WSCoL w/o UnEst are taken as comparisons. As shown in Fig. 6 (a), WSCoL is better than the other two comparisons while the three methods gradually increase in mAP.

Hyper-parameters sensitivity. In this part, we discuss the impact of the two hyperparameters, including α in objective \mathcal{L}_{WSCoL} and the memory bank’s storage length D , under the adaptation scenario of Cityscapes \rightarrow FoggyCityscapes. As shown in Fig. 6 (b)-Top, our model can maintain relatively stable results over a wide range of α (0.4~0.7). As shown in Fig. 6 (b)-Bottom, a lower or higher value of D will lead to a mAP decreasing. This phenomenon meets our expectations. Small D suffers from insufficient information, while large D introduces excessive noise.

Conclusion

For the weak-to-strong augmentation widely used in the Mean Teacher framework is the core mechanism to generate rich while contrasting visual semantics. However, this augmentation scheme suffers a inherent problem of losing crucial visual components, blocking the learning converge to cross-domain features. In this paper, a new WSCoL approach is introduced to tackle this issues. Considering that the weak augmentation is a semantics lossless operation, we conduct a weak-to-strong learning in an optimal shared space with three pivot designs. The first is the mapping network identifying the shared space gradually. The other two are the adaptation-aware prototype-guided clustering (refining auxiliary information from the weak features) and the cross-category contrastive learning with uncertainty estimation (promoting the cross-domain features extraction). Extensive experiments confirm the effectiveness of our method.

Supplementary Material for Rethinking Weak-to-Strong Augmentation in Source-Free Domain Adaptive Object Detection

Jiuzheng Yang¹, Song Tang^{1,2*}, Yangkuiyi Zhang¹, Shuaifeng Li³,
Mao Ye³, Jianwei Zhang², Xiatian Zhu⁴

¹University of Shanghai for Science and Technology ²Universität Hamburg

³University of Electronic Science and Technology of China ⁴University of Surrey

eason1337@gmail.com, tangs@usst.edu.cn, maoye@uestc.edu.cn, xiatian.zhu@surrey.ac.uk

Datasets

We evaluated the proposed method on five tasks, building on seven datasets listed below.

- **Cityscapes** (Cordts et al. 2016) dataset includes 2,975 training images and 500 test images captured under normal weather conditions, with annotations for 8 categories.
- **Foggy-Cityscapes** (Sakaridis, Dai, and Van Gool 2018) simulates foggy conditions using images from Cityscapes and retains the same annotations. For the adaptation task Cityscapes \rightarrow Foggy-cityscapes, we following the common setup (Li et al. 2022), only use the most severe foggy condition (0.02) for model training and evaluation.
- **Pascal** (Everingham et al. 2010) is a dataset of natural images containing 20 categories, we follow the standard data split as described in (Saito et al. 2019), selecting the training and validation sets from PASCAL VOC 2007 and 2012 as the source domain, which together include 16,551 images.
- **Clipart** (Inoue et al. 2018) contains 1,000 clipart-style images across the same 20 categories as Pascal, with 500 images allocated for training and 500 for testing. For the adaptation task Pascal \rightarrow Clipart, We utilize training and testing image to train and test our model correspondingly, where the source model was trained on Pascal.
- **Watercolor**(Inoue et al. 2018) dataset consists of 1K training images and 1K testing images across six categories. For the adaptation task Pascal \rightarrow Watercolor, we follow the common setup (Li et al. 2022), training the source model using only the six categories shared between the Pascal and Watercolor datasets.
- **KITTI** (Geiger et al. 2013) dataset contains 7,481 urban images that differ from typical urban scenes and are used to train the source detector model, with Cityscapes as the target domain. For the adaptation task KITTI \rightarrow Cityscapes, we following the common setup (Li et al. 2022), using the model trained on all source data to detect the car category in the target domain (Cityscapes).
- **Sim10K** (Johnson-Roberson et al. 2016) is a synthetic dataset obtained from the video game Grand Theft Auto V (GTA5), containing 10K images of the car category with 58,701 bounding boxes. For the adaptation task Sim10k \rightarrow Cityscapes, we report the performance on the car category as a common setting in the target domain (Cityscapes).

Structure of Mapping Network

Conv $2048 \times 3 \times 3$, stride 2 \rightarrow BatchNorm \rightarrow ReLU
Conv $1024 \times 3 \times 3$, stride 2 \rightarrow BatchNorm \rightarrow ReLU
Conv $1024 \times 3 \times 3$, stride 2 \rightarrow BatchNorm \rightarrow ReLU
FC (1024, 2048) \rightarrow BatchNorm \rightarrow ReLU
FC (2048, 2048) \rightarrow BatchNorm \rightarrow ReLU
FC (2048, 512)

Table 5: Architectures of the Mapping network.

Implementation details

Provision of test code. The test code is provided in the supplementary material. The link to the complete code will be provided after publication of this article.

Training setting. For the sake of fairness, we follow the experimental setting of previous work (Li et al. 2022; VS, Oza, and Patel 2023), where Faster RCNN is adopted as the base detector. The backbone network is ResNet (He et al. 2016) pre-trained on ImageNet (Russakovsky et al. 2015). In all experiments, the shorter side of each input image is resized to 600 pixels. For the proposed framework, the EMA momentum rate for the teacher network is set to 0.9 and the numbers of teacher proposals is set to $M = 300$. Additionally, the high-confidence threshold generated by the teacher network is set to 0.9. The student model is trained using SGD optimizer with the learning rate of 0.001 and the momentum of 0.9. We report the mean Average Precision (mAP) of the teacher network on the target domain with an IoU threshold of 0.5 during test. All experiments were implemented on a single 4090 GPU using the PyTorch and Detectron2 detection frameworks, with a batch size of 1 and trained for 10 epochs.

Network setting. For *Urban Scene Adaptation* (Cityscapes \rightarrow FoggyCityscapes, Sim10k \rightarrow Cityscapes, and KITTI \rightarrow Cityscapes), we use ResNet50 as our backbone. For *Image Style Adaptation* (Pascal \rightarrow Watercolor and Pascal \rightarrow Clipart), we use ResNet101.

Augmentations. For *Urban Scene Adaptation*, consistent with previous works (Li et al. 2021; Chu et al. 2023; VS, Oza, and Patel 2023; Deng, Li, and Duan 2024), we use techniques such as mosaic as strong augmentations. For *Image Style Adaptation*, we leverage style enhancement in LODS (Li et al. 2022) as strong augmentations. The weak augmentations

Pascal → Clipart																						
Method	SF	aero	bicycle	bird	boat	bottle	bus	car	cat	chair	cow	table	dog	horse	bike	prsn	plnt	sheep	sofa	train	tv	mAP
Source	-	26.8	28.8	23.4	24.1	41.9	31.4	28.5	4.9	32.0	11.0	29.8	4.3	41.2	53.3	43.7	42.0	13.1	19.9	37.1	34.4	28.6
SWDA	✗	26.2	48.5	32.6	33.7	38.5	54.3	37.1	18.6	34.8	58.3	17.0	12.5	33.8	65.5	61.6	52.0	9.3	24.9	54.1	49.1	38.1
SAPNet	✗	27.4	70.8	32.0	27.9	42.4	63.5	47.5	14.3	48.2	46.1	31.8	17.9	43.8	68.0	68.1	49.0	18.7	20.4	55.8	51.3	42.2
PD	✗	41.5	52.7	34.5	28.1	43.7	58.5	41.8	15.3	40.1	54.4	26.7	28.5	37.7	75.4	63.7	48.7	16.5	30.8	54.5	48.7	42.1
UMT	✗	39.6	59.1	32.4	35.0	45.1	61.9	48.4	7.5	46.0	67.6	21.4	29.5	48.2	75.9	70.5	56.7	25.9	28.9	39.4	43.6	44.1
SOAP	✓	34.6	46.7	26.8	23.2	34.9	33.5	39.3	16.5	29.1	33.6	17.9	12.0	26.9	41.2	37.1	34.5	14.3	23.4	36.3	35.7	29.9
LODS	✓	43.1	61.4	40.1	36.8	48.2	45.8	48.3	20.4	44.8	53.3	32.5	26.1	40.6	86.3	68.5	48.9	25.4	33.2	44.0	56.5	45.2
IRG	✓	20.3	47.3	27.3	19.7	30.5	54.2	36.2	20.6	35.1	20.6	20.2	12.3	28.7	53.1	47.5	42.4	9.1	21.1	42.3	50.3	31.5
WScOL	✓	42.8	57.2	34.9	43.2	41.5	78.9	44.7	3.0	50.8	54.0	40.1	19.6	48.7	88.2	61.2	46.5	30.3	43.0	52.6	46.2	46.4

Table 6: Full of results on task Pascal → Clipart.

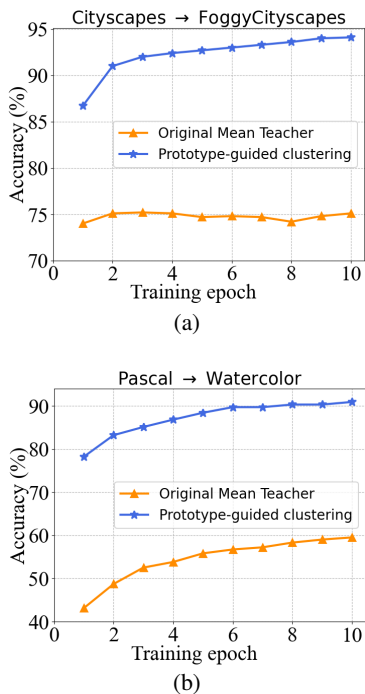


Figure 7: The comparison of classification accuracy of foreground instances on (a) Cityscapes → Foggy Cityscapes and (b) Pascal → Watercolor.

include resizing and horizontal flipping.

Parameter setting. The parameter α in $\mathcal{L}_{\text{WScOL}}$ is set to 0.5 on all datasets. The threshold of uncertainty estimation u is specified to 20.0. The temperature parameter of contrastive learning is set to $\tau = 0.07$. The size and EMA weight of the memory bank is set to $D = 10$ and $\eta = 0.4$, respectively.

Initialization and structure of Mapping network. For the initialization problem of Θ_{MNet} , we implement a gradual transition during the first epoch of training. Initially, we cluster the features \bar{x} and \bar{z} separately. The final pseudo-labels are then determined by combining the distances $D_{\text{cos}(\bar{x})}$ and $D_{\text{cos}(\bar{z})}$ from the two clusters using a weighted sum: $\bar{y} = \arg \min_j ((1-t) \times D_{\text{cos}(\bar{x})} + t \times D_{\text{cos}(\bar{z})})$, where t

denotes the proportion of the current iteration within the first epoch. The architecture of the MNet is shown in Table 5.

More quantitative results

Full results of Pascal → Clipart. Tab. 6 is the supplement of average results on task Pascal → Clipart (reported in Tab. 6), displaying the full detection results over the 20 categories. Specifically, WScOL totally obtain best results on half categories, leading to the advantage on average accuracy. On some cases, such as chair, sofa, train and sheep, WScOL has presents significant advantages over the previous methods.

Analysis of the effectiveness of prototype-guided clustering. To evaluate effectiveness of the adaptation-aware prototype-guided clustering, we conducted a quantitative analysis on Cityscapes → Foggy Cityscapes and Pascal → Watercolor, as presented in Fig. 7. Specifically, we compared the classification accuracy of foreground instances in proposals (with an IoU greater than 0.5 against the ground truth) across the two tasks. Meanwhile, the accuracy obtained by the original Mean Teacher method is taken as comparison. The results demonstrate that our clustering method can effectively extract valuable information from weak samples.

Error bar analysis. To facilitate the reproduction of experimental results, we use a fixed randomly generated random seed 17731508 in all experiments. In order to analyze the error bars introduced by this, WScOL is run under four random seeds, and the average and standard deviation of the results of the five seeds are calculated, as shown in Tab. 7. The results show that our method can obtain stable results under different random seeds.

More Qualitative analysis

Qualitative Comparison. To qualitatively verify our methods, we visualize the detection results on Pascal → Watercolor (Fig. 8), Pascal → clipart (Fig. 9) and Cityscapes → Foggy Cityscapes (Fig. 10). Obviously, our method is capable of detecting more objects while maintaining accuracy. Furthermore, we observe that our method is able to effectively detect targets even when only partial information is available. These results indicate that our WScOL lets detector to learn crucial category-related information.

Pascal → Watercolor							
Method/seed	17731508 (default)	48270820	35416060	18077346	32617189	Mean	Standard deviation
WSCoL	60.7	61.0	60.5	60.6	60.3	60.62	0.21

Table 7: Error bars on **Pascal** → **Watercolor**. Five quantitative results from one default seed 17731508 and other four randomly generated seeds are displayed.

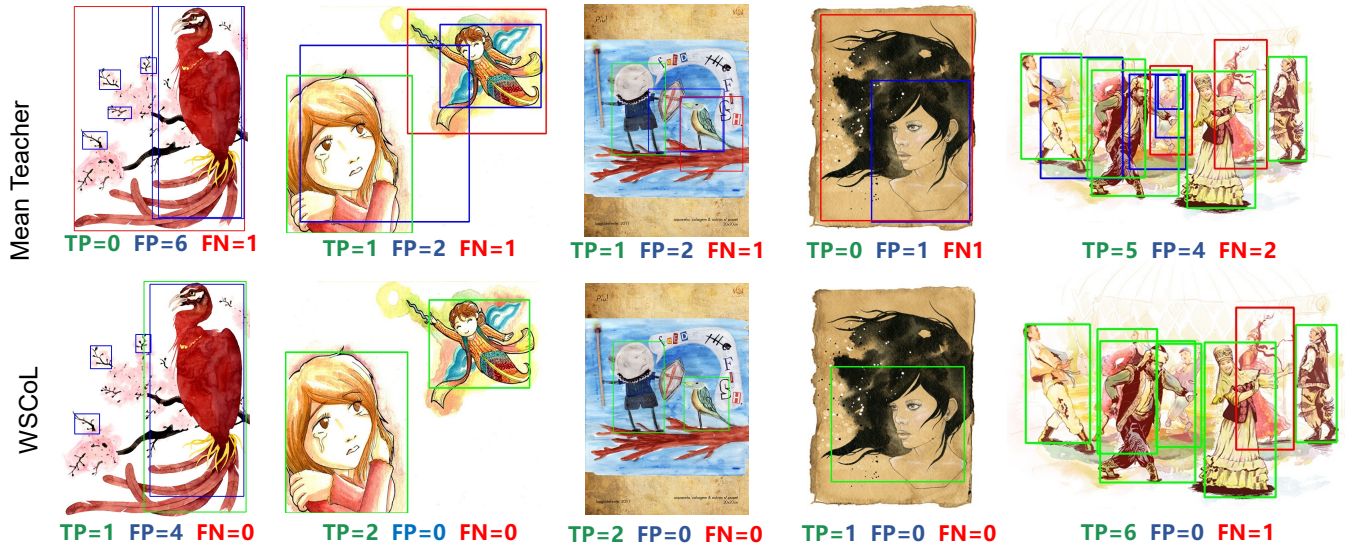


Figure 8: Quantitative results of Mean Teacher and our WSCoL on Pascal → Watercolor. Green, blue and red boxes represent true positives (TP), false positives (FP), and false negatives (FN) respectively. *Zoom in for best view.*

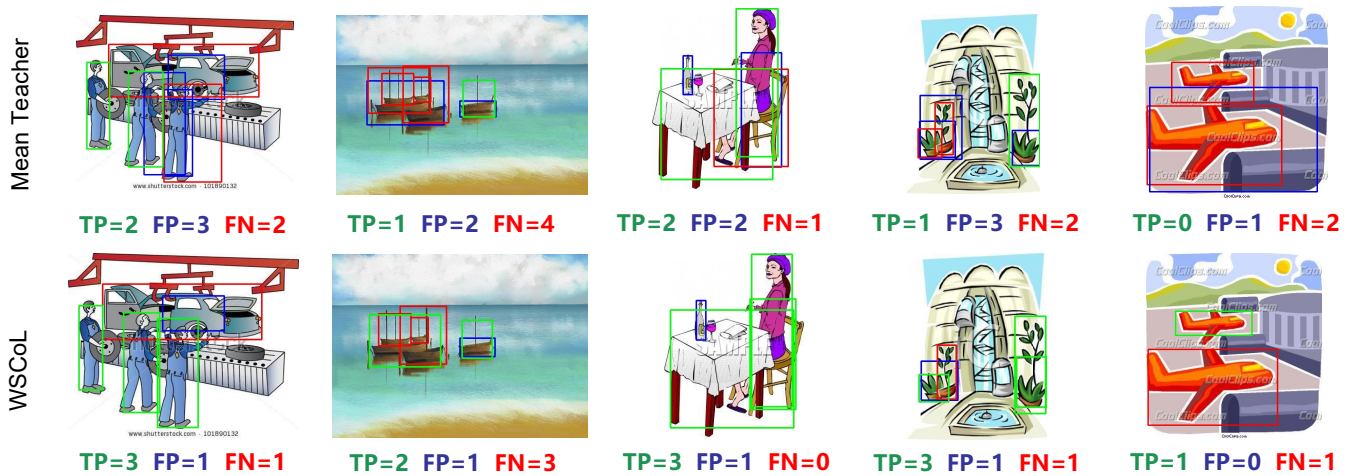


Figure 9: Quantitative results on Pascal → Clipart. Green, blue and red boxes represent true positives (TP), false positives (FP), and false negatives (FN) respectively. *Zoom in for best view.*

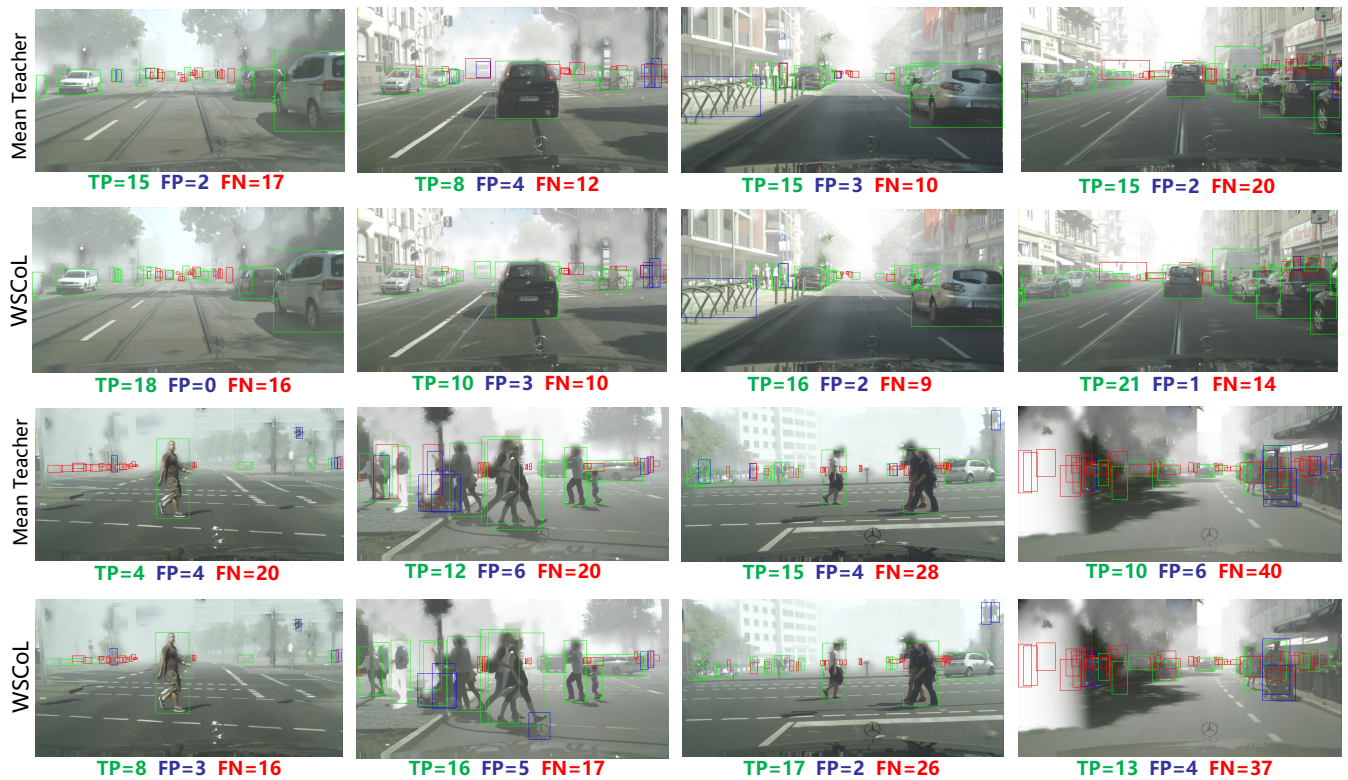


Figure 10: Quantitative results on Cityscapes \rightarrow Foggy Cityscapes. Green, blue and red boxes represent true positives (TP), false positives (FP), and false negatives (FN) respectively. *Zoom in for best view.*

References

- Bochkovskiy, A.; Wang, C.-Y.; and Liao, H.-Y. M. 2020. Yolov4: Optimal speed and accuracy of object detection. *arXiv preprint arXiv:2004.10934*.
- Cai, Q.; Pan, Y.; Ngo, C.-W.; Tian, X.; Duan, L.; and Yao, T. 2019. Exploring object relation in mean teacher for cross-domain detection. In *Proceedings of the IEEE/CVF Conference on Computer Vision and Pattern Recognition*, 11457–11466.
- Chen, C.; Zheng, Z.; Ding, X.; Huang, Y.; and Dou, Q. 2020a. Harmonizing transferability and discriminability for adapting object detectors. In *Proceedings of the IEEE/CVF conference on computer vision and pattern recognition*, 8869–8878.
- Chen, T.; Kornblith, S.; Norouzi, M.; and Hinton, G. 2020b. A Simple Framework for Contrastive Learning of Visual Representations. *arXiv:2002.05709*.
- Chen, Y.; Li, W.; Sakaridis, C.; Dai, D.; and Van Gool, L. 2018. Domain adaptive faster r-cnn for object detection in the wild. In *Proceedings of the IEEE conference on computer vision and pattern recognition*, 3339–3348.
- Chen, Z.; Wang, Z.; and Zhang, Y. 2023. Exploiting low-confidence pseudo-labels for source-free object detection. In *Proceedings of the 31st ACM International Conference on Multimedia*, 5370–5379.
- Chu, Q.; Li, S.; Chen, G.; Li, K.; and Li, X. 2023. Adversarial alignment for source free object detection. In *Proceedings of the AAAI Conference on Artificial Intelligence*, volume 37, 452–460.
- Cordts, M.; Omran, M.; Ramos, S.; Rehfeld, T.; Enzweiler, M.; Benenson, R.; Franke, U.; Roth, S.; and Schiele, B. 2016. The cityscapes dataset for semantic urban scene understanding. In *Proceedings of the IEEE conference on computer vision and pattern recognition*, 3213–3223.
- Deng, J.; Li, W.; Chen, Y.; and Duan, L. 2021. Unbiased mean teacher for cross-domain object detection. In *Proceedings of the IEEE/CVF Conference on Computer Vision and Pattern Recognition*, 4091–4101.
- Deng, J.; Li, W.; and Duan, L. 2024. Balanced Teacher for Source-free Object Detection. *IEEE Transactions on Circuits and Systems for Video Technology*.
- Du, Y.; Yang, H.; Chen, M.; Jiang, J.; Luo, H.; and Wang, C. 2021. Generation, augmentation, and alignment: A pseudo-source domain based method for source-free domain adaptation. *arXiv:2109.04015*.
- Everingham, M.; Van Gool, L.; Williams, C. K.; Winn, J.; and Zisserman, A. 2010. The pascal visual object classes (voc) challenge. *International journal of computer vision*, 88: 303–338.
- Ganin, Y.; Ustinova, E.; Ajakan, H.; Germain, P.; Larochelle, H.; Laviolette, F.; Marchand, M.; and Lempitsky, V. 2016. Domain-Adversarial Training of Neural Networks. *arXiv:1505.07818*.
- Geiger, A.; Lenz, P.; Stiller, C.; and Urtasun, R. 2013. Vision meets robotics: The kitti dataset. *The International Journal of Robotics Research*, 32(11): 1231–1237.
- He, K.; Fan, H.; Wu, Y.; Xie, S.; and Girshick, R. 2020. Momentum Contrast for Unsupervised Visual Representation Learning. *arXiv:1911.05722*.
- He, K.; Zhang, X.; Ren, S.; and Sun, J. 2016. Deep residual learning for image recognition. In *Proceedings of the IEEE conference on computer vision and pattern recognition*, 770–778.
- Hsu, C.-C.; Tsai, Y.-H.; Lin, Y.-Y.; and Yang, M.-H. 2020a. Every pixel matters: Center-aware feature alignment for domain adaptive object detector. In *Computer Vision—ECCV 2020: 16th European Conference, Glasgow, UK, August 23–28, 2020, Proceedings, Part IX 16*, 733–748. Springer.
- Hsu, H.-K.; Yao, C.-H.; Tsai, Y.-H.; Hung, W.-C.; Tseng, H.-Y.; Singh, M.; and Yang, M.-H. 2020b. Progressive domain adaptation for object detection. In *Proceedings of the IEEE/CVF winter conference on applications of computer vision*, 749–757.
- Inoue, N.; Furuta, R.; Yamasaki, T.; and Aizawa, K. 2018. Cross-domain weakly-supervised object detection through progressive domain adaptation. In *Proceedings of the IEEE conference on computer vision and pattern recognition*, 5001–5009.
- Johnson-Roberson, M.; Barto, C.; Mehta, R.; Sridhar, S. N.; Rosaen, K.; and Vasudevan, R. 2016. Driving in the matrix: Can virtual worlds replace human-generated annotations for real world tasks? *arXiv preprint arXiv:1610.01983*.
- Khodabandeh, M.; Vahdat, A.; Ranjbar, M.; and Macready, W. G. 2019. A robust learning approach to domain adaptive object detection. In *Proceedings of the IEEE/CVF International Conference on Computer Vision*, 480–490.
- Khosla, P.; Teterwak, P.; Wang, C.; Sarna, A.; Tian, Y.; Isola, P.; Maschinot, A.; Liu, C.; and Krishnan, D. 2020. Supervised contrastive learning. *Advances in neural information processing systems*, 33: 18661–18673.
- Kim, T.; Jeong, M.; Kim, S.; Choi, S.; and Kim, C. 2019. Diversify and match: A domain adaptive representation learning paradigm for object detection. In *Proceedings of the IEEE/CVF Conference on Computer Vision and Pattern Recognition*, 12456–12465.
- Lao, Q.; Jiang, X.; and Havaei, M. 2020. Hypothesis Disparity Regularized Mutual Information Maximization. *arXiv:2012.08072*.
- Li, C.; Du, D.; Zhang, L.; Wen, L.; Luo, T.; Wu, Y.; and Zhu, P. 2020a. Spatial attention pyramid network for unsupervised domain adaptation. In *Computer Vision—ECCV 2020: 16th European Conference, Glasgow, UK, August 23–28, 2020, Proceedings, Part XIII 16*, 481–497. Springer.
- Li, R.; Jiao, Q.; Cao, W.; Wong, H.-S.; and Wu, S. 2020b. Model Adaptation: Unsupervised Domain Adaptation Without Source Data. In *2020 IEEE/CVF Conference on Computer Vision and Pattern Recognition (CVPR)*, 9638–9647.
- Li, S.; Ye, M.; Zhu, X.; Zhou, L.; and Xiong, L. 2022. Source-free object detection by learning to overlook domain style. In *Proceedings of the IEEE/CVF Conference on Computer Vision and Pattern Recognition*, 8014–8023.

- Li, X.; Chen, W.; Xie, D.; Yang, S.; Yuan, P.; Pu, S.; and Zhuang, Y. 2021. A free lunch for unsupervised domain adaptive object detection without source data. In *Proceedings of the AAAI Conference on Artificial Intelligence*, volume 35, 8474–8481.
- Liu, Q.; Lin, L.; Shen, Z.; and Yang, Z. 2023. Periodically exchange teacher-student for source-free object detection. In *Proceedings of the IEEE/CVF International Conference on Computer Vision*, 6414–6424.
- Ren, S.; He, K.; Girshick, R.; and Sun, J. 2015. Faster r-cnn: Towards real-time object detection with region proposal networks. *Advances in neural information processing systems*, 28.
- Rodriguez, A. L.; and Mikolajczyk, K. 2019. Domain adaptation for object detection via style consistency. *arXiv preprint arXiv:1911.10033*.
- RoyChowdhury, A.; Chakrabarty, P.; Singh, A.; Jin, S.; Jiang, H.; Cao, L.; and Learned-Miller, E. 2019. Automatic adaptation of object detectors to new domains using self-training. In *Proceedings of the IEEE/CVF Conference on Computer Vision and Pattern Recognition*, 780–790.
- Russakovsky, O.; Deng, J.; Su, H.; Krause, J.; Satheesh, S.; Ma, S.; Huang, Z.; Karpathy, A.; Khosla, A.; Bernstein, M.; et al. 2015. Imagenet large scale visual recognition challenge. *International journal of computer vision*, 115: 211–252.
- Saito, K.; Ushiku, Y.; Harada, T.; and Saenko, K. 2019. Strong-weak distribution alignment for adaptive object detection. In *Proceedings of the IEEE/CVF conference on computer vision and pattern recognition*, 6956–6965.
- Sakaridis, C.; Dai, D.; and Van Gool, L. 2018. Semantic foggy scene understanding with synthetic data. *International Journal of Computer Vision*, 126: 973–992.
- Sindagi, V. A.; Oza, P.; Yasarla, R.; and Patel, V. M. 2020. Prior-based domain adaptive object detection for hazy and rainy conditions. In *Computer Vision–ECCV 2020: 16th European Conference, Glasgow, UK, August 23–28, 2020, Proceedings, Part XIV 16*, 763–780. Springer.
- Tang, S.; Chang, A.; Zhang, F.; Zhu, X.; Ye, M.; and Zhang, C. 2024a. Source-free domain adaptation via target prediction distribution searching. *International journal of computer vision*, 132(3): 654–672.
- Tang, S.; Su, W.; Ye, M.; and Zhu, X. 2024b. Source-Free Domain Adaptation with Frozen Multimodal Foundation Model. In *Proceedings of the IEEE/CVF Conference on Computer Vision and Pattern Recognition*, 23711–23720.
- Tang, S.; Zou, Y.; Song, Z.; Lyu, J.; Chen, L.; Ye, M.; Zhong, S.; and Zhang, J. 2022. Semantic consistency learning on manifold for source data-free unsupervised domain adaptation. *Neural Networks*, 152: 467–478.
- Tanwisuth, K.; Fan, X.; Zheng, H.; Zhang, S.; Zhang, H.; Chen, B.; and Zhou, M. 2021. A Prototype-Oriented Framework for Unsupervised Domain Adaptation. *arXiv:2110.12024*.
- Tarvainen, A.; and Valpola, H. 2017. Mean teachers are better role models: Weight-averaged consistency targets improve semi-supervised deep learning results. *Advances in neural information processing systems*, 30.
- Tian, J.; Zhang, J.; Li, W.; and Xu, D. 2021. VDM-DA: Virtual Domain Modeling for Source Data-free Domain Adaptation. *arXiv:2103.14357*.
- Vs, V.; Gupta, V.; Oza, P.; Sindagi, V. A.; and Patel, V. M. 2021. Mega-cda: Memory guided attention for category-aware unsupervised domain adaptive object detection. In *Proceedings of the IEEE/CVF Conference on Computer Vision and Pattern Recognition*, 4516–4526.
- VS, V.; Oza, P.; and Patel, V. M. 2023. Instance relation graph guided source-free domain adaptive object detection. In *Proceedings of the IEEE/CVF Conference on Computer Vision and Pattern Recognition*, 3520–3530.
- Wu, A.; Han, Y.; Zhu, L.; and Yang, Y. 2021. Instance-invariant domain adaptive object detection via progressive disentanglement. *IEEE Transactions on Pattern Analysis and Machine Intelligence*, 44(8): 4178–4193.
- Xiong, L.; Ye, M.; Zhang, D.; Gan, Y.; Li, X.; and Zhu, Y. 2021. Source data-free domain adaptation of object detector through domain-specific perturbation. *International Journal of Intelligent Systems*, 36(8): 3746–3766.
- Yang, S.; Wang, Y.; van de Weijer, J.; Herranz, L.; and Jui, S. 2021. Exploiting the Intrinsic Neighborhood Structure for Source-free Domain Adaptation. *arXiv:2110.04202*.
- Zhang, D.; Li, J.; Xiong, L.; Lin, L.; Ye, M.; and Yang, S. 2019. Cycle-consistent domain adaptive faster RCNN. *IEEE Access*, 7: 123903–123911.
- Zhou, L.; Li, N.; Ye, M.; Zhu, X.; and Tang, S. 2024. Source-free domain adaptation with Class Prototype Discovery. *Pattern Recognition*, 145: 109974.
- Zhu, X.; Pang, J.; Yang, C.; Shi, J.; and Lin, D. 2019. Adapting object detectors via selective cross-domain alignment. In *Proceedings of the IEEE/CVF Conference on Computer Vision and Pattern Recognition*, 687–696.